PROJECT TITLE: Temporal Dystrophic Remodeling within the Intrinsic Cardiac Nervous System of the Streptozotocin Diabetic Rat Model

STUDENT NAME: Chantalle Menard **SUPERVISORS:** Drs. Rakesh Arora and Paul Fernyhough

DEPARTMENT AFFILIATION: Institute of Cardiac Sciences

SUMMARY:

There is significant evixdence to support the existence of "diabetic cardiomyopathy," described as heart failure (HF) in diabetic individuals in the absence of obstructive coronary disease and hypertension. The underlying pathogenesis is only partially understood, but alterations in the autonomic nervous system's (ANS) control of cardiac function have been implicated. An important component of the cardiac ANS is the intrinsic cardiac nervous system (ICNS). The ICNS behaves as a neuronal modulator of cardiac function, and has been called the "little brain on the heart". While there have been several investigations into the effects of diabetes on extracardiac neurons, little is known about the alterations that occur in the ICNS. It is proposed that high glucose concentrations induce toxicity via oxidative stress, resulting in neuronal dystrophy and dysfunction. Our first aim was therefore to confirm that a process of dystrophic remodeling occurs within the ICNS of diabetic hearts. Our second aim was to examine the role of oxidative stress in the pathogenesis of neuronal dystrophy. Our preliminary data indicated that neuronal dystrophy occurs in the ICNS neurons of streptozotocin (STZ)-diabetic rats, and accumulates temporally within the disease process. It was also determined that an increase in reactive oxygen species (ROS) occurs in the neuronal processes of diabetic rats, indicating an association between oxidative stress and the development of a dystrophy. While our preliminary work provides novel insight for diabetes and cardiac research, more investigations are needed to further examine neuronal dysfunction and cell death, and to prove a causative role for oxidative stress in the development of dystrophy.

ACKNOWLEDGEMENTS:
Melanie Durston, Melanie Ngo, Aresh Sepehri, Donald Chapman, Dr. Elena Zherebitskaya, Dr. Gordon Glazner, and Dr. Yun Li.
The St. Boniface General Hospital Research Foundation provided the student's stipend.
The Dr. Arora's research is supported by grants from SBRF, MHRC, URGP, and the University of Manitoba Department of Surgery

Student: _____ **Supervisors:** _____

_____

1. Introduction

The prevalence of diabetes is increasing at an alarming rate, paralleling the trends of heart failure (HF)[1,2]. It is estimated that the global number of people with diabetes will increase from 135 million in 1995 to 380 million by 2025[3-6]. While the relationship between heart failure and diabetes can be partially explained by the concomitant risk factors associated with diabetes, significant evidence now exists to support diabetes as a separate risk factor for HF[4-9]. HF associated with diabetes mellitus, or "diabetic cardiomyopathy" is unique in that it occurs in the absence of both obstructive coronary artery disease (CAD) and hypertension[4,7,8,10].

The correlation between diabetic cardiomyopathy (DC) and the development of HF is profound. The Framingham Study found the risk of developing HF to be two times higher in diabetic males, and five times higher in diabetic females, independent of hypertension, age, CAD, obesity and hyperlipidemia[2,5,6]. Additionally, studies have shown that diabetes may be used as a prognostic indicator in HF patients[11,12], with the five-year mortality rate in patients with diabetic autonomic neuropathy having been reported to be as high as 53%, versus 15% with normal autonomic function[13-16]. The underlying pathogenesis of DC is only partly understood, but recent evidence suggests a link between autonomic dysfunction and abnormal myocardial function (heart rate and myocardial blood flow[10]) in type-1 and type-2 diabetes.

Diabetic autonomic neuropathy is a significant clinical complication of diabetes that carries substantial patient mortality and morbidity[13,14,17,18]. Cardiac function is tightly regulated by the autonomic nervous system. Classically, the autonomic nervous system has been described as containing only two neuronal effector arms: the sympathetic (SNS) and parasympathetic nervous systems (PNS). The SNS functions as an "accelerator" system, producing norepinephrine to increase heart rate and myocardial contraction force. In contrast, the PNS acts as a "brake", releasing acetylcholine to reduce cardiac performance[19-21]. The efferent postganglionic neurons of the PNS and SNS have been traditionally thought to operate in a simple relay fashion to control heart rate, but data now demonstrates that the mammalian heart possesses a complex nervous system, the intrinsic cardiac nervous system (ICNS), which can function independently to regulate the heart[22-24].

The ICNS is an important component of the cardiac autonomic nervous system. *In vivo* analysis of animal and human models have shown that intracardiac neuronal ganglia of the ICNS regulates cardiac output on a real-time, beat-to-beat basis, independent of extracardiac inputs (i.e. from the paravertebal ganglia)[22,23,25-27]. As such, the ICNS behaves as a potent neuronal modulator of cardiac function and has been called the *"little brain on the heart"*[24,28]. The ICNS contains afferent neurons[21,29], sympathetic efferent postganglionic neurons[30-32], parasympathetic efferent postganglionic neurons[33], and a large population of local circuitry neurons that perform interconnections within the intrinsic cardiac ganglionated plexuses[30,34]. The characterization of the neurons within the ICNS has been performed on both large[21,31,35-37] and small[38-41] animals, as well as the human heart[42-44]. Importantly, the human ICNS behaves in a very similar fashion to that observed in animal models[27,45]. Given its importance, alteration of ICNS function is thought to play a central role in the pathophysiology of heart failure and arrhythmias[15,46,47]. While enlarged dystrophic neuronal processes in abdominal[48,49] and sensory ganglia[50] characterize the alterations of extracardiac neurons in diabetes, very little is known of the impact of diabetes on the ICNS.

Dystrophic changes in axonal and dendritic morphology, such as neurite swellings, aberrant neurite branching, and decreased neurite outgrowth, in the absence of significant neuronal loss, are the neuropathological hallmark of diabetic neuropathy[18,51-53]. The underlying process involved in the development of dystrophic and dysfunctional neurons has yet to be established, but it has been suggested that high glucose concentrations induce toxicity and trigger diabetic neuropathy through loss or alteration of nerve fibers[54,55]. One possible culprit for the proposed toxicity is an increased level of reactive oxygen species (ROS). Cultured adult rat dorsal root ganglion neurons (DRG - a component of the sensory peripheral nervous system) exposed to high physiological concentrations of glucose,

increase production of ROS, specifically in axons. Increased levels of ROS distally place the axon under oxidative stress, manifesting in axonal swelling and degeneration, but not in cell death[50].

Hypothesis: The ICNS is remodeled in rodent model of type-1 diabetes. This remodeling is associated with increased levels of ROS that lead to progressive neuronal changes over time.

Study Aims: 1.To determine whether exposure to high glucose results in dysmorphic phenotype (i.e. undergo remodeling), indicative of neuronal dysfunction, in the ICNS of streptozotocin (STZ)-induced diabetic rats. 2. To determine if evidence of oxidative stress exists in the neurites of diabetic neurons, which may serve a causative role in the pathological alterations observed in diabetic ICNS neurons.

Model Rationale: The use of a rat model has several advantages, including its availability and low cost. Additionally, the location of the normal rat ICNS has already been previously described to be near the central portion of the atrium, consisting of three or four large ganglia, each with up to several hundred neurons, interconnected by a continuous plexus of nerve trunks, forming a ring encircling the pulmonary veins [40,56]. Most importantly, the impact of diabetes on the ICNS neurons of rats has yet to be established at length, and as such, our work serves to provide a new vantage point to the ongoing research in diabetic autonomic neuropathy.

2. Materials and Methods

2.1 Preparation of Cover Slips One day prior to cell isolation, sterile 22 mm coverslips (VWR, Mississauga, ON) were placed in 6-well culture plates and washed 3X with 2ml of 1XPBS. The coverslips were coated in 1.5ml of 0.5mg/ml poly-DL-polyornithine (PORN) (Sigma-Aldrich, St. Louise, MO) and placed in a 37°C incubator overnight. On the morning of the isolation, the PORN was removed and the coverslips were washed with Ham's F-12 nutrient mixture medium (F12 - Invitrogen, Carlsbad, CA). The coverslips were then coated with 1.5ml of 1µg/ml laminin (Nunclon Surface, Ottawa, ON, Canada) in F12 medium for 3 hours at a 37°C. The laminin was removed and the cover slips washed 3X with F12 medium just prior to the addition of the cells.

2.2 Preparation of Growth Medium The growth medium used for our neuronal culture consisted of Ham's F12 medium, plus several additives. The optimum concentration of neurotrophic factors added was determined through several experiments involving the culture of ICNS neurons from dissected adult Sprague-Dawley rats in varying concentrations of neurotrophic factors; low, medium, and high[50]. The "medium" concentration of neurotrophic factors was shown to promote the most neuronal growth, while also keeping the growth of non-neuronal cells to a level that did not interfere with neuronal analysis. The neurotrophic factors were 0.3ng/ml of nerve growth factor beta (NGF-ß - Sigma-Aldrich, St. Louise, MO), 1ng/ml of Neurotrophin-3 (NT-3 - Sigma-Aldrich, St. Louise, MO), and 5ng/ml of glial derived neurotrophic factor (GDNF - Sigma-Aldrich, St. Louise, MO). The stock N2 additive was prepared in F12 medium without antibiotic, and was composed of progesterone (Sigma-Aldrich, St. Louise, MO), putrescine (Sigma-Aldrich, St. Louise, MO), sodium selenite (Sigma-Aldrich, St. Louise, MO), fatty-acid free BSA powder (Sigma-Aldrich, St. Louise, MO), and transferrin (Sigma-Aldrich, St. Louise, MO). 40µl of stock N2 was added per 4 ml of growth medium, bringing the final concentrations to 20nM of progesterone, 100µM of putrescine, 30nM of sodium selinite, 0.1mg/ml of BSA and 100µg/ml of transferrin. To this standard growth medium, either 0.1nM of insulin, or 15mM of glucose, was added to the control and diabetic growth mediums, respectively.

2.3 Primary Cell Culture Primary cells were isolated from the hearts of adult Sprague-Dawley male rats. Rats were age matched controlled or 3- to 6-month streptozotocin (STZ)-diabetic rats. Rats were

made diabetic with a single intraperitoneal injection of 75mg/kg STZ (Sigma-Aldrich, St. Louise, MO). STZ is selectively toxic to the beta cells in the pancreatic islets. Treatment with STZ results in insulin deficiency and hyperglycemia, producing a model of type-1 diabetes. Body weight, plasma glucose and HbA1c was collected and used as endpoints for the development of diabetes. Rats were deeply anesthetized with 5% isofluorane and killed by decapitation. Hearts were removed and placed in cold 1XPBS. Using micro-dissection tools, the atria was separated from the ventricles, the great vessels, and the atrial appendages, isolating the ICNS ganglionated plexus located within the dorsal fat of the central portion of the atria, near the pulmonary veins[40,56,57]. The isolated tissue was transferred to a dish containing cold filtered 1XPBS, and surgical scissors were used to cut the tissue into small pieces. The tissue was then placed through two digestions; the first, consisting of 0.5% (w/v) collagenase (Worthington Biochemical, Lakewood, NJ) in 2mL of warm F12 medium, and the second consisting of 0.25% (w/v) trypsin (Worthington) in 2mL warm F12 medium. Both 1hr digestions were completed in a shaking incubator at 200 rpm and 37°C, with a wash of warm F12 performed in between. Following the second digestion, 1ml of fetal bovine serum (FBS) was added to deactivate the trypsin. 2ml of F12 medium was added to the cell suspension and titruated using a smoothened Pasteur pipette. The supernatant was decanted into a sterile tube and this procedure was repeated, and the collected cell suspension was passed through a 70µm cell filter into a sterile 50ml falcon tube. The filtered cell suspension was then transferred to a sterile 15ml falcon tube and centrifuged at 99.68 x g at room temperature (RT) for 5 minutes. The pellet was then resuspended in 1ml of F12 media, and added to a 1ml solution of 15% BSA (O.5ml F12 and 0.5ml 30% BSA - Sigma-Aldrich, St. Louise, MO), which was then centrifuged at 99.68 x g for 10 minutes. The pellet was resuspended in 1ml of appropriate growth medium (diabetic or control), and 150µl of the cell suspension was added to the pre-treated cover slips in the 6-well cell culture plates. The plates were then placed in an incubator for 1 hour at 37°C and 5% CO_2, after which point 1.5ml of the appropriate growth medium was added to the wells, and the plates were returned to the incubator. Cells were visualized after 48 and 72 hours of growth using a phase contrast microscope (Nikon Eclipse TS100).

2.4 Immunohistochemistry After 72 hours, the neurons were fixed with 4% paraformaldehyde in phosphate buffer at pH 7.4 for 15 min, followed by permeabilizing with 0.3% Triton X-100 in PBS. Nonspecific binding was blocked by incubation with Blocking Reagent (Roche, Indianapolis, IN) combined with FBS and 1.0M PBS in proportions of 3:1:1 for 1 hr at room temperature, followed by three washes with PBS. The coverslips were incubated in polyclonal antibody to (E)-4-hydroxy-2-nonenal (1:500 anti-4-HNE adducts Pab; Alexis Biochemicals, San Diego, CA) overnight at 4ºC in a humidified chamber. The next day, coverslips were washed several times in 1XPBS, followed by incubation in Alexa Flour 488 (Molecular Probes, Burlington, ON; 1:700) secondary antibody for 3hr at room temperature. The coverslips were washed again in 1XPBS, and incubated with polyclonal anti-protein gene product (PGP) 9.5 (1:500 – UltraClone Limited, Isle of Wight, England) overnight at 4ºC in a humidified chamber in the dark. The coverslips were then washed in 1XPBS, and then incubated for three hours with Alexa Fluor 546 (1:700). Coverslips were mounted to microscope slides using mounting medium with DAPI, Hard Set (Vector, Cat#H-1500). A Carl Zeiss LSM510 inverted confocal microscope was utilized for identification of neurons throughout specimens. Confocal images were captured using a Plan-Neofluar 40x/1.3 Oil DIC objective at 10µm intervals ascending from the substrate though neuronal cell bodies and processes (Z sections). The images were reconstructed in three dimensions using Zeiss LSM Image Browser software (Germany).

2.5 Morphometric Analysis The confocal images captured were analyzed in a blinded fashion to exclude bias. Area of neurite outgrowth, the number of branch points, and the number of neurite swellings were determined with a morphometric approach using ImageJ 1.42 software (available at http://rsbweb.nih.gov/ij/) on masked images[58]. In brief, fluorescence images of PGP staining

immunoreactive neurons were separated from their surroundings by thresholding, the cell body was deleted from the image, and measurements were made to score the immunoreactive area within the pixel range[50,58,59]. Individual neurite swellings and branch points were manually labeled and counted for each neuron[50]. Individual neurons were also classified as non-dystrophic, mildly or highly dystrophic, according to defined morphological features (see Results)[59]. More than 200 neurons were scored per experimental condition.

2.6 4-HNE Adduct Analysis The confocal images captured were analyzed with ImageJ 1.42 software in a blinded fashion to exclude bias. In brief, fluorescence images of 4-HNE adduct staining immunoreactive neurons were separated from their surroundings by thresholding, the cell body was deleted from the image, and measurements were made to score both the immunoreactive area within the pixel range and the intensity of the fluorescence. The average intensity of fluorescence was then divided by the average area of fluorescence.

2.7 Data Analysis All data, except the dystrophic neuron proportions, was subject to standard two-tailed unpaired Student's *t*-Test with significance levels of p=0.05, which does not assume equal variances, using GraphPad Prism 4 (GraphPad Prism 4, GraphPad Software Inc., San Diego, CA)[50]. All results are expressed as means ± SEM. The data for the dystrophic neuron proportions was compared using a normal approximation method.

3. Results

3.1 Primary Neuronal Cell Culture Data Phase contrast images (Fig. 1) were taken of cultured STZ-diabetic and age matched control neurons at 48 hrs of culture. Neurons were assessed for morphology and confluence. As previously demonstrated in mouse ICNS cultures[60], three different neuronal types were found to have been isolated by evaluating cell morphology, including pseudounipolar neurons (cells with a large cell body and single long neurite), bipolar neurons (spindle-shaped cells with long neurites at opposite ends), and multipolar neurons (exhibiting several neurites of various lengths) (Fig 1). The presence of nonneuronal cells (i.e. cardiac fibroblasts) was evident in cocultures, but their growth was kept to an optimal level due to our culture technique and carefully selected growth medium cocktail.

3.2 Morphometric Analysis Data Two different methods of analysis were undertaken to determine the morphology of the neurons in culture. One method assessed area of neurite outgrowth, neurite branching and neurite swellings to quantify dystrophic features[50]. The 3-month STZ-diabetic rats showed statistically significant increases in both total area (Fig. 3A) and number of neurite swellings (Fig. 3B), at, respectively, 1.2X (p=0.0042) and 1.3X (p=0.01) that of the 3-month control rats. However, neurite branching was not significantly different between culture groups (Fig. 3C). The 6-month STZ-diabetic rat neurons showed a dramatic decrease in area of neurite outgrowth (Fig. 3D), having only 0.48X (p=<0.001) the control neuron's area. The difference in the number of neurite swellings was not found to be statistically significant (Fig. 3E), but the diabetic rat neurons exhibited a significant increase in neurite branching as compared to controls, with 1.56X (p=0.0015) the number of branch points (Fig. 3F).

Secondly, defined morphological features were used to categorize the neuronal cells into three different groups, according to the degree of dystrophy; non-dystrophic, mildly dystrophic and highly dystrophic[59] (Fig. 4). Non-dystrophic neurons had a normal appearance, with smooth and intact processes (Fig. 4A). Mildly dystrophic neurons exhibited some features of dystrophy, such as sharp angles in neuronal processes, and outgrowth of lamellipodia-like structures from cell bodies and proximal neurites (arrows, Fig. 4B), while highly dystrophic neurons demonstrated highly irregular

morphological features, such as aberrant neuritic growth from cell bodies and the appearance of frequent loops and curls in neuritic processes (arrows, Fig. 4C)[59]. The 3-month STZ-diabetic rat neurons were found to be significantly more dystrophic than the 3-month control rat neurons, with higher proportions of both mildly dystrophic (34.9% vs. 21.1%, p=0.0244) and highly dystrophic (53.2% vs. 29.5%, p=0.004) neurons (Fig. 5A). There was also a higher proportion of any dystrophy (mild or high) in the diabetic neurons as compared to controls (88.1% vs. 50.5%, p=<0.0001; Fig. 5B). The 6-month STZ-diabetic rat neurons were also found to have higher proportions of mildly dystrophic neurons (39.4% vs. 27.4%, p=0.008), and while there was no significant trend in the proportions of highly dystrophic neurons at 6 months, there was still a significantly higher proportion of any dystrophy (mild or high) in diabetic neurons as compared to control neurons (74.3% vs. 62.2%, p=0.0448).

3.3 4-HNE Adduct Data At 3 months, diabetic neurons and control neurons showed no significant difference in the intensity of staining for 4-HNE adducts (Fig. 7A). However, by 6 months, the diabetic neurons showed a significant increase in intensity, with an intensity level that was 2.22X (p=<0.001) that of the control neurons (Fig. 7D). It was also noted that the intensity of 4-HNE adduct staining was increased within the neurite swellings themselves (Fig. 7B and D).

4. Discussion

4.1 Primary Neuronal Cell Cultures This study demonstrated that intrinsic cardiac neurons from adult STZ-diabetic and age-matched control rats can be maintained in culture, and that ICNS neurons show varied morphology, indicative of the cell types that exist with *in vivo* cardiac ganglia. It was also demonstrated that ICNS neuronal cells form neurite processes in culture that contact other cells. The connections made between non-neuronal cells and neuronal cells in culture are likely very important, as it has been previously demonstrated in cultures of mouse ICNS that non-neuronal cells were necessary to support neurite outgrowth[60].

4.2 Morphometric Analysis of Dystrophic Features Our first method of analyzing dystrophy involved comparing certain dystrophic features on individual neurons. Analysis of the 3 month data indicated that only one quantifiable dystrophic feature, the number of neurite swellings, was significantly greater in the diabetic neurons. Neurite swellings, thought to be the residues of aberrant intra-ganglionic sprouting, may be axonal or dendritic in nature, and have been described as being large accumulations of small mitochondria and neuronal structural proteins[18,50-52]. As specific staining was not done to differentiate axons from dendrites, all swellings observed on neuronal extensions will be referred to here as neurite swellings. The significance of neurite swellings in the pathogenesis of neuronal dysfunction may be two-fold. Firstly, the collection of debris may reflect or induce alterations in axonal transport. Altered axonal transport may result in death of mitochondria and the absence of structural proteins at distal sites. In the absence of structural proteins and ATP-generating organelles, the distal axon, lacking the sufficient tools for plasticity, is predisposed to dissolution and degeneration upon subsequent injury or stress[18,50]. Secondly, the collection of mitochondria themselves may produce a local exaggeration of oxidative stress via the overproduction of superoxide by the electron transport chain in the mitochondrial, leading to a self-propagating pathway of neuritic dystrophy [18,61]. In accordance with this view, the neurite swellings were seen to fluorescence at a greater intensity with the 4-HNE adduct staining (See section 4.3 and Fig. 6).

At 6 months, there was an increase in the number of dystrophic features observed in the diabetic group, with two of the quantifiable dystrophic features, the area of neuronal outgrowth and neurite branching, being significantly different from controls. The 6-month neurons exhibited an increase in neurite branching. Increased neurite branching has been postulated as a compensatory response of a

neuron to a loss of synapses occurring along their length[62,63]. An aberrant increase in branching morphology has also been observed in neurons affected with Alzheimer's disease (AD), characterized by a pattern of ineffective intensive growth[63]. Given the parallels that have been drawn between the effects of AD and diabetes on neurons, it is possible that this type of neurite branching may also be occurring in diabetic neurons[64-66]. Futhermore, increased neurite branching has been described in diabetic rat neurons of prevertebral and paravertebral sympathetic ganglionia[53]. In these circumstances, the aberrant branching was stimulated by an increase in the levels of nerve growth factor (NGF) within the diabetic neuron. Therefore, it was postulated that excessive amounts of neurotrophic factors may induce uncontrolled neuritic branching[67]. In diabetic neurons, the development of axonal sprouts appears to serve as a substrate for further dystrophic changes, with their appearance preceding the development of axonal swellings [53,68].

The dramatic decrease in area of neurite outgrowth observed in our 6-month diabetic neurons to less than half that of the control neurons was in stark contrast to the increase in area of neurite outgrowth observed in the diabetics at 3 months. However, given that the 3 month diabetic neurons had a much higher proportion of highly dystrophic neurons than the control group (53.2% vs. 29.5%), we postulate that at 3 months, one of the reasons that the diabetic neurons had a larger area measurement may be to increased dysmorphology, as evidence by the many loops that occurred in the neurites (Fig. 2A). At 6 months, the decrease in area of neuronal outgrowth as compared to controls is an expected and often observed finding in dystrophic diabetic neurons, owing to the degeneration of axons and nerve fiber loss[51,69,70]. The number of neurite swellings did not differ significantly between the 6-month diabetic and control neuronal groups.

A limitation of our analysis is the lack of measurement of cell-death, and this will be the subject of an ongoing investigation. However, analysis of 3-month and 6-month data demonstrated an increase in the dystrophic features in the diabetic neurons between the two time points, with two of the dystrophic features being more prominent in the 6-month diabetics, compared to only one feature for the 3-month diabetics. Importantly, it has been demonstrated in other diabetic rat peripheral neurons that the dystrophic effects of diabetes accumulates temporally, with dysmorphology progressing from mild at early time points to more pronounced at later time points[69]. Given the temporal relationship between our two experimental groups, our data is in agreement with these findings.

Due to the observed tortuosity in the neuronal processes, we performed a confirmatory analysis of dystrophic phenotype for the ICNS neurons. The classification of neurons into dystrophic or non-dystrophic categories was undertaken so as to compare neurons as a whole[59]. Importantly, at both time points, there was a significantly higher proportion of any dystrophy (mild or high) in the diabetic neurons. That the 6-month diabetic group did not exhibit a significantly greater proportion of highly dystrophic neurons was not an expected result, and may have been a feature of the study group itself. A possible explanation is that age itself produces similar dystrophic changes in neuronal morphology[49]. Thus, further investigation of alterations at the 6-month time point will be the subject of forthcoming investigations.

4.3 4-HNE Adduct Staining Several studies have confirmed staining for the presence of 4-HNE adducts as a marker for oxidative stress [50,58,71,72]. 4-HNE adducts are produced via oxidative stress dependent-lipid peroxidation, and it has been proposed that oxidative stress plays an important role in the formation of diabetes-associated dystrophic neuronal features[58,71]. Given the significant increase in the intensity of staining for 4-HNE adducts in the 6-month diabetic neurons, our study provides evidence to support this theory. Although the 3-month diabetic neurons did not show a difference in staining intensity compared to the control group, this does speak to the aforementioned increase in dystrophy that is seen to occur temporally in diabetes[69]. As stated previously, another important finding in our study was the increased intensity of staining for 4-HNE adducts that was observed inside the

neurite swellings (Fig. 6), which supports the notion that oxidative stress is associated with the formation of dystrophic features in diabetic neurons[58,61].

5.0 Conclusion Our study demonstrated for the first time in ICNS neurons of STZ-diabetic rats that dystrophic features accumulate temporally in diabetic neurons, and that features associated with neuronal oxidative stress are observed with the development of dystrophy. Our study also challenged the notion that the measurement of total area of neuronal outgrowth is a sufficient measure of neuronal outgrowth. Given the observed tortuosity of neuronal processes, additional methods for neurite outgrowth assessments, such as the length of the longest axon, might be more informative. While this preliminary data adds novel information to the field of both diabetic cardiac and neuronal research, further research is required to confirm that oxidative stress plays a causative role in dystrophic changes, and to evaluate whether the dystrophic changes observed in diabetic rat ICNS neurons leads to dysfunction or cell death. These could be assessed through experimentation with anti-oxidants, neuronal conductivity studies, and analysis of neuronal cell death. Additional work will also be necessary to further characterize the observed neurite swellings as axonal or dendritic, and to confirm the contents of the neurite swellings. As well, the branch points observed on the neurons could be assessed for NGF content to draw definitive conclusions of their significance.

6.0 References

1. Ho, K.K., Anderson, K.M., Kannel, W.B., Grossman, W. & Levy, D. Survival after the onset of congestive heart failure in Framingham Heart Study subjects. *Circulation* **88**, 107-115 (1993).
2. Ho, K.K., Pinsky, J.L., Kannel, W.B. & Levy, D. The epidemiology of heart failure: the Framingham Study. *J Am Coll Cardiol* **22**, 6A-13A (1993).
3. King, H., Aubert, R.E. & Herman, W.H. Global burden of diabetes, 1995-2025: prevalence, numerical estimates, and projections. *Diabetes Care* **21**, 1414-1431 (1998).
4. Khavandi, K.*, et al.* Diabetic cardiomyopathy--a distinct disease? *Best Pract Res Clin Endocrinol Metab* **23**, 347-360 (2009).
5. Kannel, W.B. & McGee, D.L. Diabetes and cardiovascular disease. The Framingham study. *JAMA* **241**, 2035-2038 (1979).
6. Kannel, W.B. & McGee, D.L. Diabetes and glucose tolerance as risk factors for cardiovascular disease: the Framingham study. *Diabetes Care* **2**, 120-126 (1979).
7. Iltis, I., Kober, F., Dalmasso, C., Cozzone, P.J. & Bernard, M. Noninvasive characterization of myocardial blood flow in diabetic, hypertensive, and diabetic-hypertensive rats using spin-labeling MRI. *Microcirculation* **12**, 607-614 (2005).
8. Hayat, S.A., Patel, B., Khattar, R.S. & Malik, R.A. Diabetic cardiomyopathy: mechanisms, diagnosis and treatment. *Clin Sci (Lond)* **107**, 539-557 (2004).
9. Liu, J.E.*, et al.* The impact of diabetes on left ventricular filling pattern in normotensive and hypertensive adults: the Strong Heart Study. *J Am Coll Cardiol* **37**, 1943-1949 (2001).
10. Scognamiglio, R.*, et al.* Myocardial dysfunction and adrenergic cardiac innervation in patients with insulin-dependent diabetes mellitus. *J Am Coll Cardiol* **31**, 404-412 (1998).
11. Shindler, D.M.*, et al.* Diabetes mellitus, a predictor of morbidity and mortality in the Studies of Left Ventricular Dysfunction (SOLVD) Trials and Registry. *Am J Cardiol* **77**, 1017-1020 (1996).
12. Berry, C., Brett, M., Stevenson, K., McMurray, J.J. & Norrie, J. Nature and prognostic importance of abnormal glucose tolerance and diabetes in acute heart failure. *Heart* **94**, 296-304 (2008).
13. Gerritsen, J.*, et al.* Impaired autonomic function is associated with increased mortality, especially in subjects with diabetes, hypertension, or a history of cardiovascular disease: the Hoorn Study. *Diabetes Care* **24**, 1793-1798 (2001).
14. Ziegler, D.*, et al.* Prediction of mortality using measures of cardiac autonomic dysfunction in the diabetic and nondiabetic population: the MONICA/KORA Augsburg Cohort Study. *Diabetes Care* **31**, 556-561 (2008).
15. Vinik, A.I., Maser, R.E., Mitchell, B.D. & Freeman, R. Diabetic autonomic neuropathy. *Diabetes Care* **26**, 1553-1579 (2003).
16. Cheng, Y.J.*, et al.* Heart rate recovery following maximal exercise testing as a predictor of cardiovascular disease and all-cause mortality in men with diabetes. *Diabetes Care* **26**, 2052-2057 (2003).
17. Rundles, R.W. Diabetic neuropathy. *Bull N Y Acad Med* **26**, 598-616 (1950).
18. Schmidt, R.E.*, et al.* Non-obese diabetic mice rapidly develop dramatic sympathetic neuritic dystrophy: a new experimental model of diabetic autonomic neuropathy. *Am J Pathol* **163**, 2077-2091 (2003).
19. Kollai, M. & Koizumi, K. Reciprocal and non-reciprocal action of the vagal and sympathetic nerves innervating the heart. *J Auton Nerv Syst* **1**, 33-52 (1979).
20. Levy, M.N., Martin, P.J. & Stuesse, S.L. Neural regulation of the heart beat. *Annu Rev Physiol* **43**, 443-453 (1981).
21. Armour, J.A. & Hopkins, D.A. Activity of in vivo canine ventricular neurons. *Am J Physiol* **258**, H326-336 (1990).
22. Ardell, J.L., Butler, C.K., Smith, F.M., Hopkins, D.A. & Armour, J.A. Activity of in vivo atrial and ventricular neurons in chronically decentralized canine hearts. *Am J Physiol* **260**, H713-721 (1991).
23. Arora, R.C., Ardell, J.L. & Armour, J.A. Cardiac Denervation and Cardiac Function. *Curr Interv Cardiol Rep* **2**, 188-195 (2000).
24. Armour, J.A. Potential clinical relevance of the 'little brain' on the mammalian heart. *Exp Physiol* **93**, 165-176 (2008).

25. Armour, J.A. Cardiac neuronal hierarchy in health and disease. *Am J Physiol Regul Integr Comp Physiol* **287**, R262-271 (2004).
26. Horackova, M. & Armour, J.A. Role of peripheral autonomic neurones in maintaining adequate cardiac function. *Cardiovasc Res* **30**, 326-335 (1995).
27. Arora, R.C., Hirsch, G.M., Johnson Hirsch, K., Hancock Friesen, C. & Armour, J.A. Function of human intrinsic cardiac neurons in situ. *Am J Physiol Regul Integr Comp Physiol* **280**, R1736-1740 (2001).
28. Armour, J.A. Myocardial ischaemia and the cardiac nervous system. *Cardiovasc Res* **41**, 41-54 (1999).
29. Cheng, Z., Powley, T.L., Schwaber, J.S. & Doyle, F.J., 3rd. Vagal afferent innervation of the atria of the rat heart reconstructed with confocal microscopy. *J Comp Neurol* **381**, 1-17 (1997).
30. Butler, C.K.*, et al.* Cardiac responses to electrical stimulation of discrete loci in canine atrial and ventricular ganglionated plexi. *Am J Physiol* **259**, H1365-1373 (1990).
31. Gagliardi, M.*, et al.* Activity of in vivo canine cardiac plexus neurons. *Am J Physiol* **255**, H789-800 (1988).
32. Hamos, J.E., Van Horn, S.C., Raczkowski, D., Uhlrich, D.J. & Sherman, S.M. Synaptic connectivity of a local circuit neurone in lateral geniculate nucleus of the cat. *Nature* **317**, 618-621 (1985).
33. Blomquist, T.M., Priola, D.V. & Romero, A.M. Source of intrinsic innervation of canine ventricles: a functional study. *Am J Physiol* **252**, H638-644 (1987).
34. Murphy, D.A., O'Blenes, S., Hanna, B.D. & Armour, J.A. Functional capacity of nicotine-sensitive canine intrinsic cardiac neurons to modify the heart. *Am J Physiol* **266**, R1127-1135 (1994).
35. Arora, R.C., Waldmann, M., Hopkins, D.A. & Armour, J.A. Porcine intrinsic cardiac ganglia. *Anat Rec A Discov Mol Cell Evol Biol* **271**, 249-258 (2003).
36. Hopkins, D.A., Gootman, P.M., Gootman, N. & Armour, J.A. Anatomy of medullary and peripheral autonomic neurons innervating the neonatal porcine heart. *J Auton Nerv Syst* **64**, 74-84 (1997).
37. Pauza, D.H., Skripka, V. & Pauziene, N. Morphology of the intrinsic cardiac nervous system in the dog: a whole-mount study employing histochemical staining with acetylcholinesterase. *Cells Tissues Organs* **172**, 297-320 (2002).
38. Pauza, D.H., Skripkiene, G., Skripka, V., Pauziene, N. & Stropus, R. Morphological study of neurons in the nerve plexus on heart base of rats and guinea pigs. *J Auton Nerv Syst* **62**, 1-12 (1997).
39. Pauziene, N., Pauza, D.H. & Stropus, R. Morphological study of the heart innervation of bats Myotis daubentoni and Eptesicus serotinus (Microchiroptera: Vespertilionidae) during hibernation. *Eur J Morphol* **38**, 195-205 (2000).
40. Richardson, R.J., Grkovic, I. & Anderson, C.R. Immunohistochemical analysis of intracardiac ganglia of the rat heart. *Cell Tissue Res* **314**, 337-350 (2003).
41. Roberts, L.A. Morphological innervation pattern of the developing rabbit heart. *Am J Anat* **190**, 370-384 (1991).
42. Pauza, D.H., Skripka, V., Pauziene, N. & Stropus, R. Morphology, distribution, and variability of the epicardiac neural ganglionated subplexuses in the human heart. *Anat Rec* **259**, 353-382 (2000).
43. Pauziene, N., Pauza, D.H. & Stropus, R. Morphology of human intracardiac nerves: an electron microscope study. *J Anat* **197 Pt 3**, 437-459 (2000).
44. Hoover, D.B.*, et al.* Localization of multiple neurotransmitters in surgically derived specimens of human atrial ganglia. *Neuroscience* **164**, 1170-1179 (2009).
45. Murphy, D.A. & Armour, J.A. Human cardiac nerve stimulation. *Ann Thorac Surg* **54**, 502-506 (1992).
46. Maser, R.E. & Lenhard, M.J. Cardiovascular autonomic neuropathy due to diabetes mellitus: clinical manifestations, consequences, and treatment. *J Clin Endocrinol Metab* **90**, 5896-5903 (2005).
47. Vinik, A.I. & Ziegler, D. Diabetic cardiovascular autonomic neuropathy. *Circulation* **115**, 387-397 (2007).
48. Duchen, L.W., Anjorin, A., Watkins, P.J. & Mackay, J.D. Pathology of autonomic neuropathy in diabetes mellitus. *Ann Intern Med* **92**, 301-303 (1980).
49. Schmidt, R.E., Plurad, S.B., Parvin, C.A. & Roth, K.A. Effect of diabetes and aging on human sympathetic autonomic ganglia. *Am J Pathol* **143**, 143-153 (1993).
50. Zherebitskaya, E., Akude, E., Smith, D.R. & Fernyhough, P. Development of selective axonopathy in adult sensory neurons isolated from diabetic rats: role of glucose-induced oxidative stress. *Diabetes* **58**, 1356-1364 (2009).

51. Schmidt, R.E. Neuropathology and pathogenesis of diabetic autonomic neuropathy. *Int Rev Neurobiol* **50**, 257-292 (2002).
52. Schmidt, R.E., Parvin, C.A. & Green, K.G. Synaptic ultrastructural alterations anticipate the development of neuroaxonal dystrophy in sympathetic ganglia of aged and diabetic mice. *J Neuropathol Exp Neurol* **67**, 1166-1186 (2008).
53. Schmidt, R.E*., et al.* Effect of streptozotocin-induced diabetes on NGF, P75(NTR) and TrkA content of prevertebral and paravertebral rat sympathetic ganglia. *Brain Res* **867**, 149-156 (2000).
54. Russell, J.W*., et al.* High glucose-induced oxidative stress and mitochondrial dysfunction in neurons. *FASEB J* **16**, 1738-1748 (2002).
55. Vincent, A.M., Brownlee, M. & Russell, J.W. Oxidative stress and programmed cell death in diabetic neuropathy. *Ann N Y Acad Sci* **959**, 368-383 (2002).
56. Horackova, M., Slavikova, J. & Byczko, Z. Postnatal development of the rat intrinsic cardiac nervous system: a confocal laser scanning microscopy study in whole-mount atria. *Tissue Cell* **32**, 377-388 (2000).
57. Horackova, M., Croll, R.P., Hopkins, D.A., Losier, A.M. & Armour, J.A. Morphological and immunohistochemical properties of primary long-term cultures of adult guinea-pig ventricular cardiomyocytes with peripheral cardiac neurons. *Tissue Cell* **28**, 411-425 (1996).
58. Jackson, A.C., Kammouni, W., Zherebitskaya, E. & Fernyhough, P. Role of oxidative stress in rabies virus infection of adult mouse dorsal root ganglion neurons. *J Virol* **84**, 4697-4705 (2010).
59. Grace, E.A., Rabiner, C.A. & Busciglio, J. Characterization of neuronal dystrophy induced by fibrillar amyloid beta: implications for Alzheimer's disease. *Neuroscience* **114**, 265-273 (2002).
60. Hoard, J.L., Hoover, D.B. & Wondergem, R. Phenotypic properties of adult mouse intrinsic cardiac neurons maintained in culture. *Am J Physiol Cell Physiol* **293**, C1875-1883 (2007).
61. Brownlee, M. Biochemistry and molecular cell biology of diabetic complications. *Nature* **414**, 813-820 (2001).
62. Dickstein, D.L., Brautigam, H., Stockton, S.D., Jr., Schmeidler, J. & Hof, P.R. Changes in dendritic complexity and spine morphology in transgenic mice expressing human wild-type tau. *Brain Struct Funct* **214**, 161-179 (2010).
63. Arendt, T., Bruckner, M.K., Bigl, V. & Marcova, L. Dendritic reorganisation in the basal forebrain under degenerative conditions and its defects in Alzheimer's disease. II. Ageing, Korsakoff's disease, Parkinson's disease, and Alzheimer's disease. *J Comp Neurol* **351**, 189-222 (1995).
64. de la Monte, S.M. & Wands, J.R. Alzheimer's disease is type 3 diabetes-evidence reviewed. *J Diabetes Sci Technol* **2**, 1101-1113 (2008).
65. de la Monte, S.M., Tong, M., Lester-Coll, N., Plater, M., Jr. & Wands, J.R. Therapeutic rescue of neurodegeneration in experimental type 3 diabetes: relevance to Alzheimer's disease. *J Alzheimers Dis* **10**, 89-109 (2006).
66. Jolivalt, C.G*., et al.* Defective insulin signaling pathway and increased glycogen synthase kinase-3 activity in the brain of diabetic mice: parallels with Alzheimer's disease and correction by insulin. *J Neurosci Res* **86**, 3265-3274 (2008).
67. Isaacson, L.G., Saffran, B.N. & Crutcher, K.A. Nerve growth factor-induced sprouting of mature, uninjured sympathetic axons. *J Comp Neurol* **326**, 327-336 (1992).
68. Schmidt, R.E. Synaptic dysplasia in sympathetic autonomic ganglia. *J Neurocytol* **25**, 777-791 (1996).
69. Kamiya, H., Zhang, W. & Sima, A.A. Dynamic changes of neuroskeletal proteins in DRGs underlie impaired axonal maturation and progressive axonal degeneration in type 1 diabetes. *Exp Diabetes Res* **2009**, 793281 (2009).
70. Schmidt, R.E. & Scharp, D.W. Axonal dystrophy in experimental diabetic autonomic neuropathy. *Diabetes* **31**, 761-770 (1982).
71. Akude, E., Zherebitskaya, E., Roy Chowdhury, S.K., Girling, K. & Fernyhough, P. 4-Hydroxy-2-nonenal induces mitochondrial dysfunction and aberrant axonal outgrowth in adult sensory neurons that mimics features of diabetic neuropathy. *Neurotox Res* **17**, 28-38 (2010).
72. Akude, E*., et al.* Diminished superoxide generation is associated with respiratory chain dysfunction and changes in the mitochondrial proteome of sensory neurons from diabetic rats. *Diabetes* **60**, 288-297 (2011).

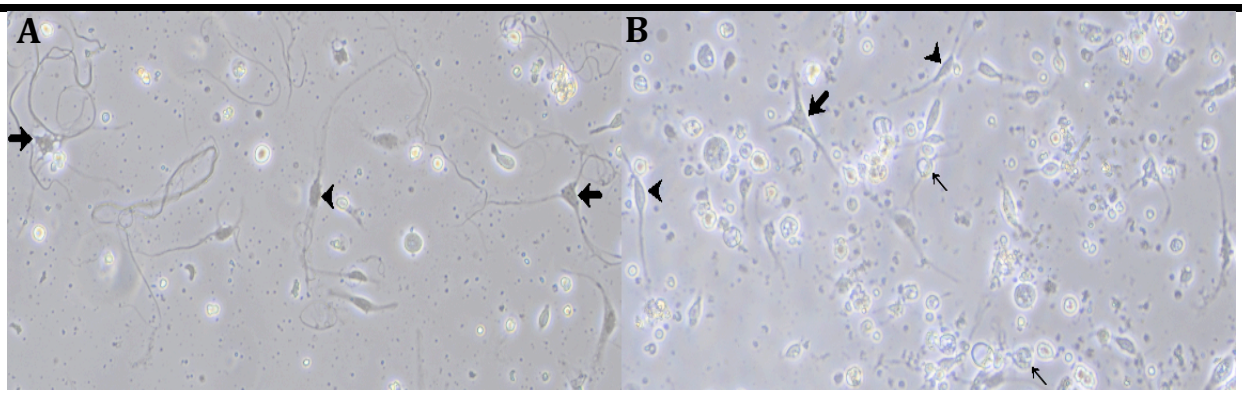

Figure 1. Intrinsic Cardiac Neuron Cultures Panels A and B are representative of normal neuronal cells in culture identified via Bright phase microscopy. Panel A demonstrates STZ-diabetic rat neurons at 48 hours in culture. Panel B demonstrates age-matched control rat neurons at 48 hours in culture. Several different neuronal types were isolated, including large pseudounipolar appearing cells similar to dorsal root ganglion cells (thin arrows), as well as bi- (arrowheads) and multi-polar (thick arrows) cells indicative of efferent or interneuronal cell types.

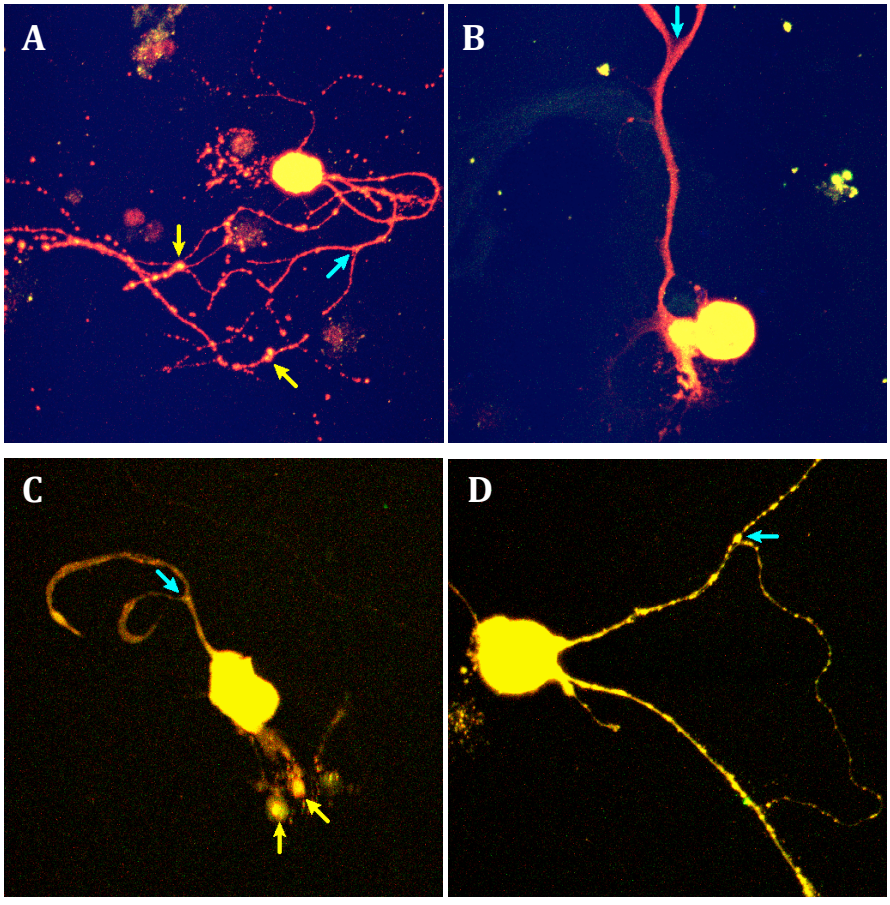

Figure 2. Immunoflourescence of Neuronal Cultures Images were captured on a Carl Zeiss LSM510 inverted confocal microscope with a 40x objective. Panels A (STZ-diabetic) and B (age-matched control) are images collected from the 3-month rat cultures, while panels C (STZ-diabetic) and D (age-matched control) are images of the 6-month rat cultures. The dystrophic feature of neurite swelling (yellow arrows) is indicated in panels A and C, and examples of neurite branching (blue arrows) can be seen in all panels.

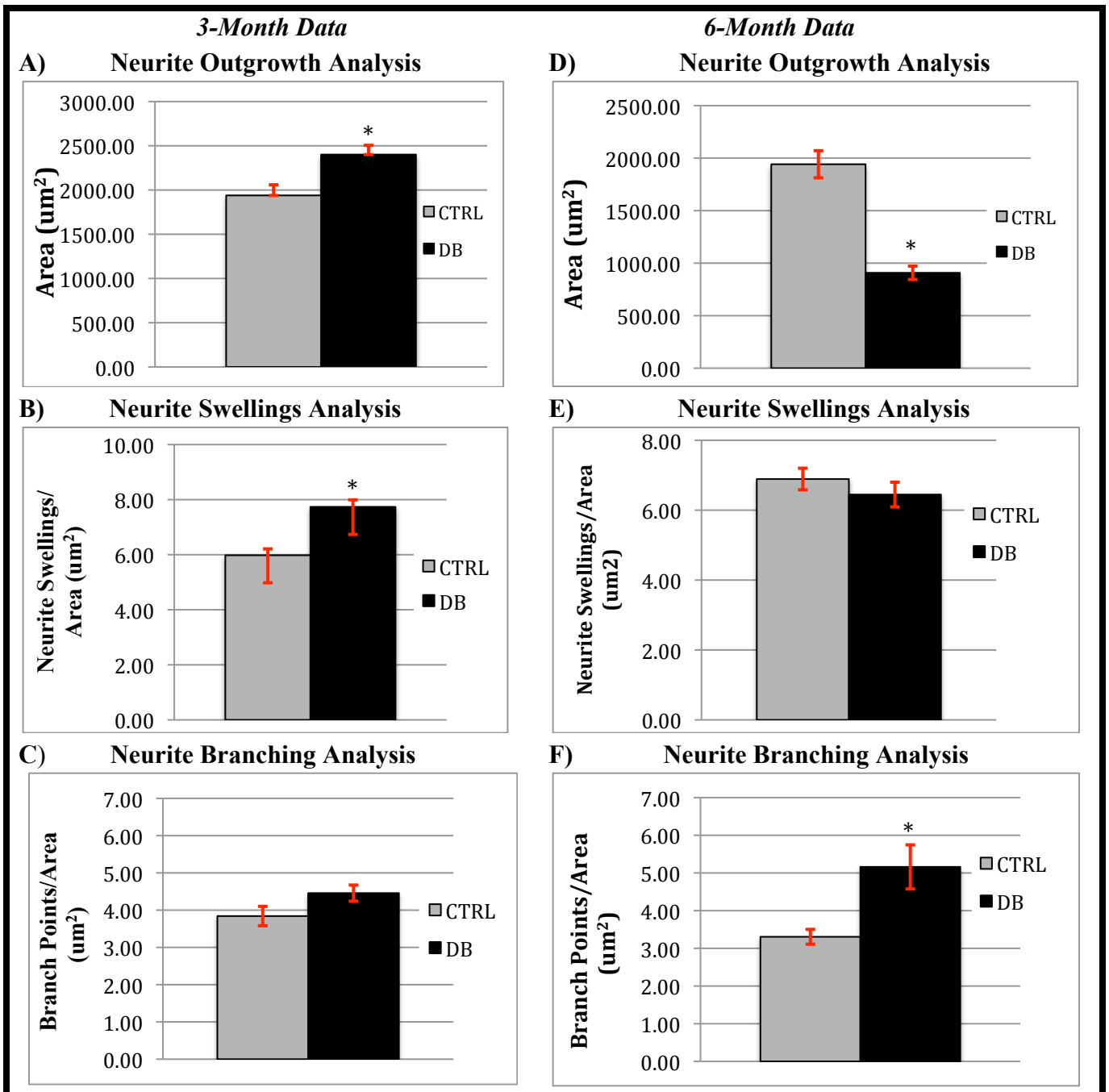

Figure 3. Neurite Outgrowth, Neurite Swellings and Neurite Branching as Measures of Dystrophy. Panels A, B, and C represent the data collected from 3-month diabetic and control rat neuronal cultures. An asterisk (*) indicates statistically significant data. Error bars indicate the mean ± the S.E.M. At 3 months, area (neuronal outgrowth) and the number of neurite swellings were both found to be significantly increased in diabetic neurons, at, respectively, 1.2X ($p=0.0042$) and 1.3X ($p=0.01$) that of control neurons. Branching was higher in diabetic neurons, although not significantly, at 1.16X the control, $p=0.0688$. Panels C, D, and E represent the data collected from 6-month diabetic and control rat neuronal cultures. At 6 months, area was found to be significantly lower in the diabetic neurons, as compared to the control neurons, at 0.48X ($p=<0.001$). While there was no significant difference between diabetic or control neurons in the amount of neurite swellings ($p=0.3438$), the diabetic neurons were seen to have a significantly higher amount of neurite branching, at 1.56X ($p=0.0015$) that of the control neurons.

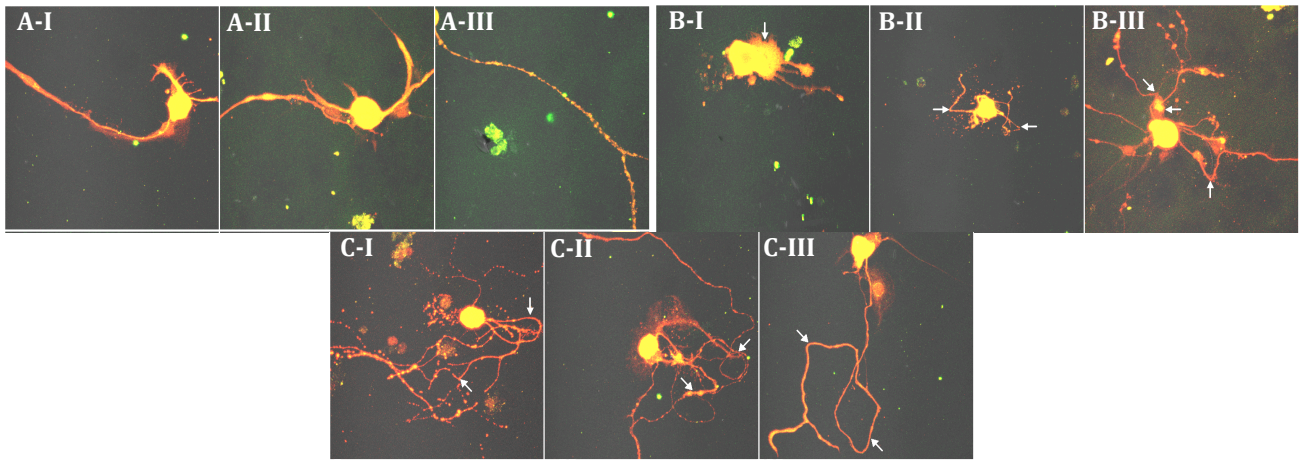

Figure 4. Quantifying dystrophic features Neurons were classified into different categories, according to the degree of dystrophy, as defined by certain morphological features. Non-dystrophic neurons had a normal appearance, with smooth and intact processes (AI-III). Mildly dystrophic neurons exhibited some features of dystrophy, such as outgrowths of lamellipodia-like structures from cell bodies and proximal neurites (arrows, BI), and sharp angles in neuronal processes (arrows, BII and III. Highly dystrophic neurons demonstrated highly irregular morphological features, such as aberrant neuritic growth from cell bodies and the appearance of frequent loops and curls in neuritic processes (arrows, CI-III).

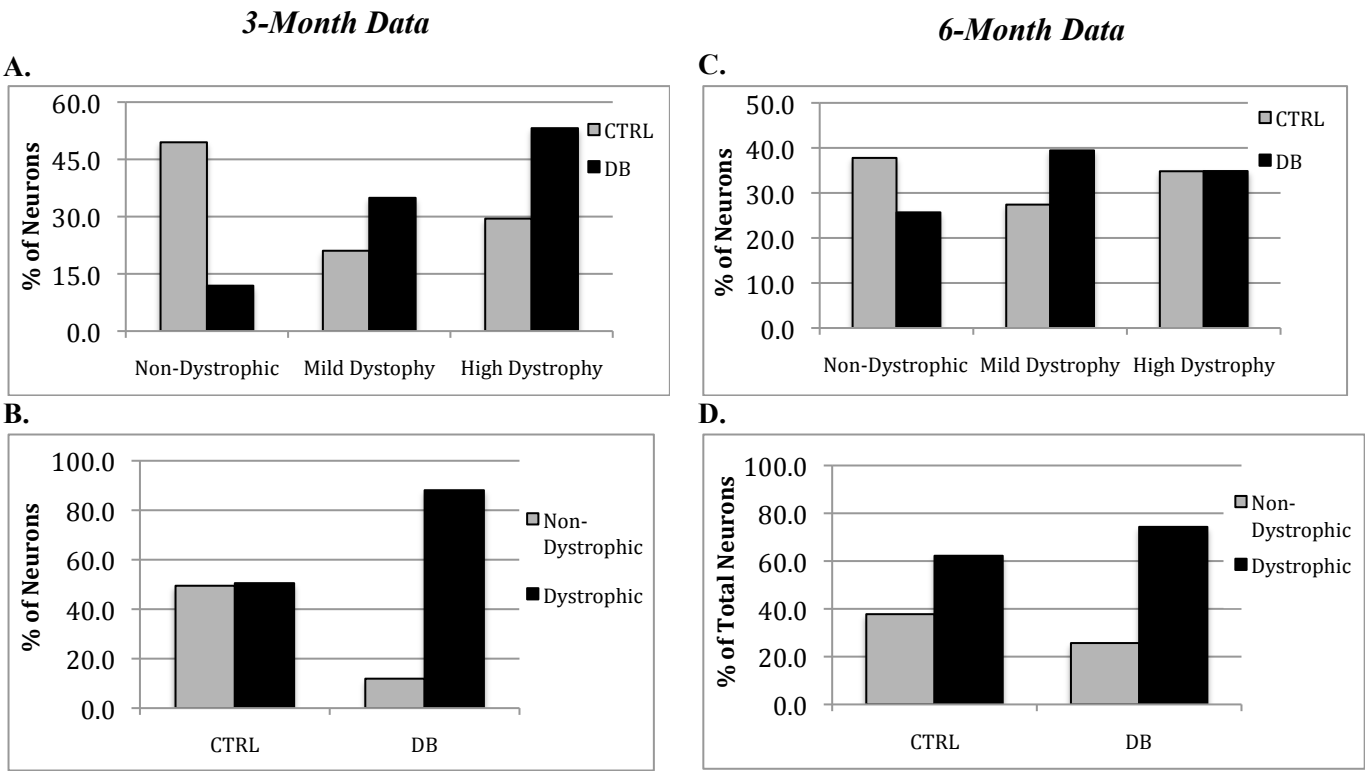

Figure 5. Morphological Assessment of Neuronal Dystrophy Panels A and B represent data collected from the 3-month neuronal cultures. As panel A indicates, at 3 months, there were significantly higher proportions of mildly (34.9% vs. 21.1%, p=0.0244) and highly dystrophy (53.2% vs. 29.5%, p=0.0004) neurons in the diabetic neurons vs. the control neurons. Panel B indicates there was a significantly higher proportion of any dystrophy (mild or high) in the diabetic vs. the control neurons (88.1% vs. 50.5%, p=<0.0001). Panels C and D represent data collected from 6-month neuronal cultures. At 6 months, there was a significantly higher proportion of mild dystrophy in diabetic neurons vs. control (39.4% vs. 27.4%, p=0.008), but no statistical significance to the proportions of neurons that were highly dystrophic. Additionally, as seen in Panel D, there was a significantly higher proportion of any dystrophy (mild or high) in the diabetic neurons vs. the controls (74.3% vs. 62.2%, p=0.0448).

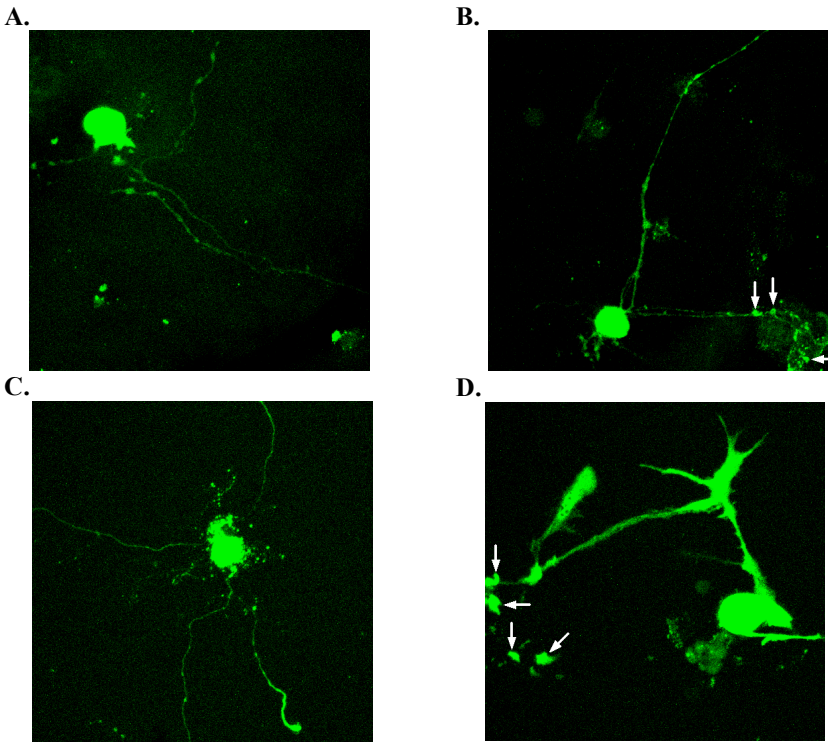

Figure 6. Immunoflourescence of 4HNE Adducts Panels A (age-matched control) and B (STZ-diabetic) are images of 3-month neuronal cultures. Panels C (aged-matched control) and D (STZ-diabetic) are images of 6-month neuronal cultures. Neurons were stained with immunoflourescence for 4-HNE adducts, and images were captured on a Carl Zeiss LSM510 inverted confocal microscope with a 40x objective. The software program ImageJ 1.42 (available at http://rsbweb.nih.gov/ij/) was used to quantify both the intensity of fluorescence, and the total neurite area staining positive for 4-HNE adducts. Note in panels C and D the increased intensity of fluorescence expressed in the neurite swellings (white arrows).

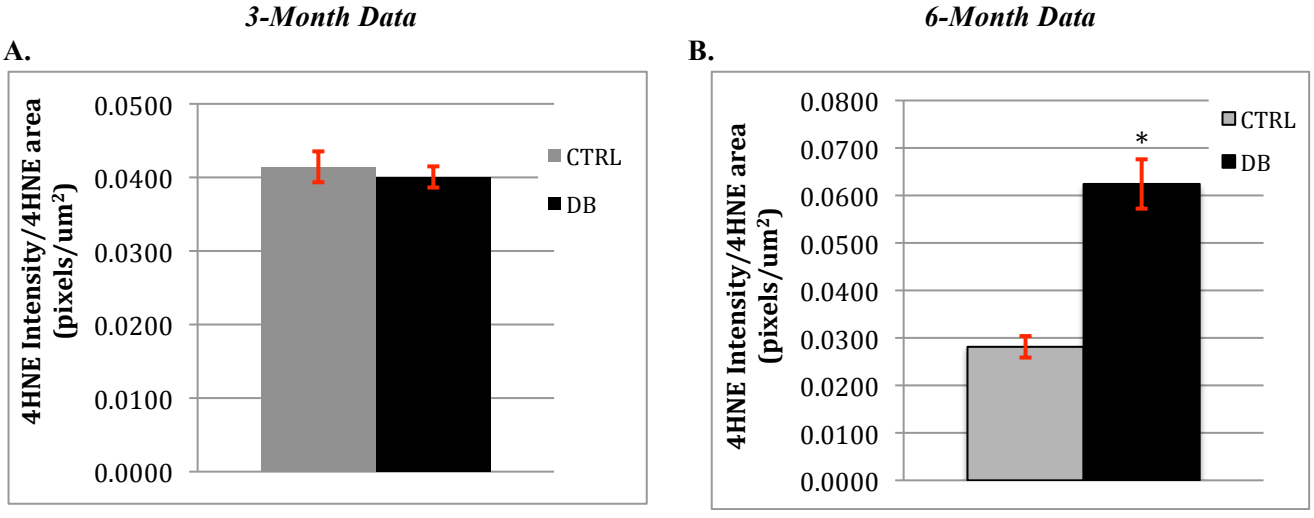

Figure 7. Intensity of 4-HNE Adduct Staining Panels A and B are the graphical representation of the fluorescence intensity recorded for 4-HNE adduct staining vs. the total 4-HNE staining neurite area for both 3- and 6-month STZ-diabetic and age-matched control rat neuronal cultures. An asterisk (*) indicates statistically significant data. Error bars indicate the mean ± the S.E.M. At 3 months (panel A), there was no statistical significance in 4-HNE adduct staining between diabetic and control neurons ($p=0.5755$). At 6 months (Panel B), there was a significant difference observed, with the diabetic neurons displaying a 4-HNE adduct staining intensity per total 4-HNE staining area that was 2.22X that seen in the controls ($p=<0.0001$).